

A comprehensive study on the effects of operation variables on reverse electro dialysis performance

Accepted Manuscript

Desalination

20 February 2020

V.M. Ortiz-Martínez, L. Gómez-Coma, C. Tristán, G. Pérez, M. Fallanza, A. Ortiz, R. Ibañez, I. Ortiz*

Department of Chemical and Biomolecular Engineering. University of Cantabria,
Av. Los Castros 46, 39005 Santander, Spain
*corresponding author: ortizi@unican.es

©2020 This manuscript version is made available under the CC-BY-NC-ND 4.0 license

<http://creativecommons.org/licenses/by-nc-nd/4.0/>

The definitive publisher version is available online at <https://doi.org/10.1016/j.desal.2020.114389>

Abstract

Despite the great prospects of reverse electrodialysis (RED), which directly transforms salinity gradient energy into electricity, new efforts focusing on its optimization are still required before large-scale implementation. RED performance is determined by numerous variables including (i) membrane properties, (ii) compartment and spacer design, (iii) stream concentrations defining salinity gradient, (iv) flow velocity and fluidodynamics. Among them, low salinity stream (LC) concentration and feed flow rates are key operation variables with great impact on power output; thus, this work approaches their parametric analysis through modeling tools. Initially, as novel study, LC salinity influence was deeply analyzed by quantifying its relative contribution to the overall internal resistance while determining the rest of all ohmic and non-ohmic components. Seawater was selected as high concentrated solution (HC), 0.55 M NaCl, due to its global availability for RED exploitation. LC and Reynolds number analysis are needed to select suitable water sources and devise new strategies to adapt RED performance. LC salinity of 0.02 M NaCl and $Re_{HC}=3.4$ and $Re_{LC}=7$ allowed to reach the highest net power density. A previously developed mathematical model was used, with simulated results validated in a laboratory-scale plant, offering valuable input for future decision-making in RED operation and upscaling.

Keywords: Blue energy; Salinity gradient (SG); RED performance; Low Concentration Solution Influence; Re number analysis.

1. Introduction

The depletion of fossil fuels together with the associated environmental impact derived from their utilization and the growing trends in global energy consumption call for the deployment of new energy sources to ensure sustainable economic growth. According to the International Renewable Energy Agency (IRENA), energy demands will increase significantly by 80 % in 2050 [1]. Salinity Gradient Power (SGP), also known as Blue Energy, is a promising option for clean and renewable energy generation whose interest has exponentially raised in the last decade [2]. SGP uses the Gibbs energy from the mixing of two water streams with different salinity. Usually, seawater has been targeted as high concentrated solution (HC) and river water as low concentrated solution (LC). Nevertheless, other water sources are possible, for instance, industrial brine solutions as HC streams, and lake, underground water and treated urban wastewater as LC streams. Previous works have reported that up to 0.8 kWh could be obtained when 1 m³ of fresh water flows into the sea [3]. In fact, the global energy output from estuaries is estimated at 2.6 TW, representing an important source for energy recovery [4,5]

Currently, two emerging technologies to harvest the SGP are being intensively investigated, pressure retarded osmosis (PRO) and reverse electrodialysis (RED). These two emission-free and sustainable options are based on the use of selectively permeable membranes. The only pilot plant based on PRO technology to date was set up in Tofte (Norway) by the company Statkraft, using seawater and river water as HC and LC streams, respectively. The initial power generation target was 10 kW and a second phase included the building of a full-scale plant of 25 MW by 2015 [6]. However, the pilot plant ceased activities in 2014 due to operational problems such as membrane fouling, among others. In fact, when PRO and RED technology have been compared, the first option has been considered a more attractive option for power generation from concentrated saline brines due to a higher energy recovery capacity [4]. On the other hand, RED technology has been proposed as a more advantageous technique to harvest SGP from the mixing of seawater and river water [7,8]. RED performance is greatly influenced by the configuration and design of the modules and several operational variables. In the last decade, there has been an exponential rise in the number of works dealing with the study of such parameters in order to assess the tradeoffs of the technology and to compare different scenarios. According to the main approach followed both in terms of experimental work and mathematical modeling, the studies can be grouped into: (i) stack

design optimization, including the analysis of the properties of ion exchange membranes (IEMs) [9–12], the role played by spacers [13,14] and electrode configuration [15,16]; (ii) module operation, covering important variables such as feed solution concentration [11,12,17,18], effect of ion species [19,20], flow rates [21], temperature [22,23] and operation mode strategies [24]; and (iii) integration of RED technology in hybrid processes [25,26]. Also, it is worth noting that the operation at pilot scale has already been demonstrated in two different scenarios. On one hand, a pilot plant using brines and brackish water was set up in Marsala (Italy), reaching power outputs of 700 W with artificial NaCl solutions and of up to 330 W with real water streams [27,28]. On the other hand, a pilot plant working with seawater and river water was built in Afsluitdijk (The Netherlands) with a target of 50 kW of gross power [29]. More recently, new strategies for water reclamation through RED technology in coastal wastewater treatment plants have been proposed [30].

In terms of stack configuration, the progress achieved in the last few years in membrane development and spacer design have made possible to greatly increase the performance of RED technology [31]. Gross power density, net power density and energy efficiency are the main outputs to quantify the performance of the RED stacks [11], which are strongly impacted by the operational variables, such as concentration and flow rate, membrane properties and stack configuration. Permselectivity and electrical resistance are the most relevant properties of IEMs, affecting power performance [32,33]. On the other hand, these two parameters are influenced by the ion exchange capacity, charged density and water content. Moreover, permselectivity is not only determined by intrinsic membrane properties, but also by surrounding conditions such as solutions concentration. Generally, high salt solution concentration can affect electrostatic exclusion decreasing IEM permselectivity [34]. Many studies have employed commercially available membranes for RED set-up, but there is an increasing trend in tailoring IEMs to optimize their performance [35]. In the same way, different spacer designs have been explored to promote suitable stream flows, to reduce the internal resistance of the compartments and to enhance the mixing in the diffusive boundary layers, including profile-membrane options [36,37].

In respect of operational variables, the feed solutions are responsible for the electromotive driving force and significantly influence the internal resistance of the stack [27,38]. In general, RED performance is improved when the salinity difference between the HC and

LC solutions is increased. However, as already mentioned, membrane permselectivity has been shown to decrease when high salt HC streams such as concentrated brines are employed, thus limiting further improvement of power generation [39]. At the same time, for a fixed HC, the variation of the LC contributes with two competing effects on electromotive force and internal resistance. In this sense, low conductivities in the LC compartments can lead to a significant negative impact on the overall resistance of the system [40]. On its part, the feed flow velocity can favor the mixing in water compartments while boosting the electromotive force and reducing the non-ohmic components of the internal resistance. However, the increase in the feed rate is achieved at the cost of increasing pumping energy, lowering the net power output [21]. These implications indicate that the influence of LC concentration and feed flow velocities of the feed streams need to be thoroughly analyzed under systematic approaches to find optimal operational conditions.

Several previous works have focused on the experimental analysis of the influence of the solutions concentration and the feed flow rates on power performance [5,27,28,37,38,41–43], employing brines or seawater as HC solutions along with river water [39,42,44–47], brackish water [27,28,43,48], wastewater [49,50] or seawater (when brines are used as high concentration solution) [43,51] as LC solutions. However, further modeling analysis is needed to deeply study the influence of these two variables over a wide range. The exhaustive analysis of the effect of the concentration in the LC compartments will lead to proper decision-making when it comes to selecting the suitable water streams as well as to devise new strategies to adapt the available ones. For example, urban treated wastewater could be employed as LC for further valorization, but they usually present low conductivity. Their salinity could be increased up to the desired concentration by being mixed with a fraction of seawater.

On the other hand, the optimal flow velocity of LC may differ from that of HC and, therefore, the parametric analysis of both rates is important to select the optimal feed solution rates that ensure maximum net power density considering pumping costs. The assessment of the RED performance as a function of the Reynolds number takes into consideration the geometry of the system and the fluid properties such as density and viscosity, and thus, it is a useful tool to study different configuration stacks and water streams for comparative purposes and upscaling.

This work delves into the optimal operational variables in terms of LC concentration and Reynolds number. On one hand, an in-depth analysis of the influence of the LC compartment was performed by determining its relative contribution to the overall internal resistance and searching for the optimal concentration of the LC stream, for a fixed concentration of 0.5 M NaCl for the HC compartment. The concentration of the HC streams was maintained because it represents the average salinity for seawater, which is the most widely employed stream as high salinity flow. On the other hand, the effect of the Reynolds number in both HC and LC compartments was systematically analyzed in terms of gross and net power, which represents an innovative approach. This study was carried out using a robust mathematical model implemented in the Aspen Custom Modeler[®] software, and the simulated results were validated in a laboratory-scale plant. While the number of operation conditions can be limited by experimental approaches, mathematical tools can help to analyze a wide range of scenarios contributing to future decision-making for RED optimization and upscaling.

2. Materials and methods

2.1. Experimental set-up

The experiments were performed using a RED stack formed of 20 cell pairs supplied by Fumatech (Fumatech[®], Germany). Specifically, the stack was equipped with the Fumasep membranes FAS-50 and FKS-50, as anion and cation exchange membranes, respectively, with 200 cm² of active membrane area. Long et al (2018) reported the highest performance of these membranes in terms of net power out and energy efficiency in comparison to other commercial membranes [11]. Commercial polyethersulfone spacers with a thickness of 270 μm, effective area of 200 cm² and porosity of 82.5% were employed to separate the membranes, while anode and cathode electrodes consisted of titanium and mixed oxides. A summary of the main specifications of the RED system as well as the representation of the laboratory plant is provided as Supplementary Material (see Table S1 and Figure S1).

The electrode rinse solution (ERS) consisted of 0.05 M K₃Fe(CN)₆, 0.05 M K₄Fe(CN)₆ (Scharlau, purity >99.0%, Spain) and 0.25 M NaCl (Fisher Chemicals, assay >99.5%, UK). ERS was continuously recirculated through the electrode compartments. Experiments were performed by using an electronic load device under galvanostatic mode

(Chroma Systems Solutions 63103A, USA). Voltage output was measured as a function of current. The RED stack was left in open circuit mode until a stable open-circuit voltage (OCV) was obtained, typically 5 min (steady-state conditions). Then, electrical current was modified in steps of 0.025 A and maintained until voltage output remained constant. For experimental tests, synthetic water streams were prepared using industrial grade sodium chloride (purity>99.5%, Fisher Chemicals, Spain) in distilled water. The stack was continuously fed with stream solutions at a constant temperature of 24 ± 1 °C.

2.2. Mathematical model

A robust mathematical model previously reported and developed in the software Aspen Custom Model V9 (AspenTech) was used to predict the electrical performance of the RED stack under several operation conditions. A detailed description of this model can be found in the work by Ortiz-Imedio et al. [52]. As a summary, this model assumes co-current flow distribution, with main variables of the system (resistances, cell pair voltage, voltage output, power and current) being evaluated at the average conditions between the inlets and outlets of the stack. Ion fluxes in the solutions are quantified through mass balance equations.

The Nernst equation was employed for determination of the cell pair voltage, according to the following expression:

$$E_{cell}(x) = \alpha_{CEM} \cdot \frac{R \cdot T}{F} \cdot \left[\frac{1}{z_i} \ln \left(\frac{\gamma_{HC}^{Na^+}(x) \cdot C_{HC}^{Na^+}(x)}{\gamma_{LC}^{Na^+}(x) \cdot C_{LC}^{Na^+}(x)} \right) \right] + \alpha_{AEM} \cdot \frac{R \cdot T}{F} \cdot \left[\frac{1}{z_{ion}} \ln \left(\frac{\gamma_{HC}^{Cl^-}(x) \cdot C_{HC}^{Cl^-}(x)}{\gamma_{LC}^{Cl^-}(x) \cdot C_{LC}^{Cl^-}(x)} \right) \right] \quad (1)$$

where α_{CEM} and α_{AEM} stand for the permselectivities of the cation and anion exchange membranes, respectively, z is the ion valence, γ is the ion activity coefficient in the solutions, C is ion concentration (mol/m^3), F is the Faraday constant (C/mol), R is the universal gas constant ($\text{J}/(\text{mol} \cdot \text{K})$) and T is temperature (K).

This model includes the estimation of the internal resistance of the stack mainly caused by ohmic and non-ohmic contributions. Specifically, the resistances of the membranes (R_m) and of the compartments (R_{HC} and R_{LC}) correspond to ohmic components, while non-ohmic resistance is due to the streamwise concentration change along the compartments

(R_{AC}) and the boundary layer resistance (R_{BL}). The voltage output (E) is given by the theoretical voltage of the stack (sum of total cell voltages) considering the internal total resistance of the system ($R_{stack}, \Omega \cdot m^2$) according to the following equation:

$$E = \sum E_{cell} - j \cdot R_{stack} \quad (2)$$

where j stands for current density (A/m^2).

Finally, the gross power density, P_{gross} (W/m^2_{mp}), was calculated considering the output voltage and the electric current (I) as well as the number of membrane pairs (N) and the effective area per membrane (A) as follows:

$$P_{gross} = \frac{E \cdot I}{(N \cdot A)} \quad (3)$$

For the characterization of the energy performance in RED stacks, the net power density (P_{net}) can be calculated by subtracting the power spent in pumping (P_{pump}) from the gross power [47] according to eq. 4.a and 4.b:

$$P_{net} (W/m^2) = \frac{E \cdot I - P_{pump}}{N \cdot A} \quad (4. a)$$

$$P_{pump} (W) = \frac{\Delta P_{HC} \cdot Q_{HC} + \Delta P_{LC} \cdot Q_{LC}}{\eta} \quad (4. b)$$

where ΔP_{HC} and ΔP_{LC} are the respective pressure drops (Pa) between the inlets and the outlets of the low and high concentration solutions, Q_{HC} and Q_{LC} are the volumetric flow rates (m^3/s) in the high and low concentration solutions, respectively, and η is the pump efficiency (set by default to 75%) [27,41]. In turn, ΔP_{HC} and ΔP_{LC} are calculated according to the pressure drop in a spacer filled system [53].

The Reynold numbers (Re) used in this study has been calculated according to eq. 5 [36,52]:

$$Re (-) = \frac{2 \cdot Q \cdot \rho}{\varepsilon \cdot b \cdot \mu} \quad (5)$$

where b is the spacer thickness (m), Q is the flow rate (m^3/s), ρ is the density of the solutions (kg/m^3) and μ is the dynamic viscosity ($kg/(m \cdot s)$).

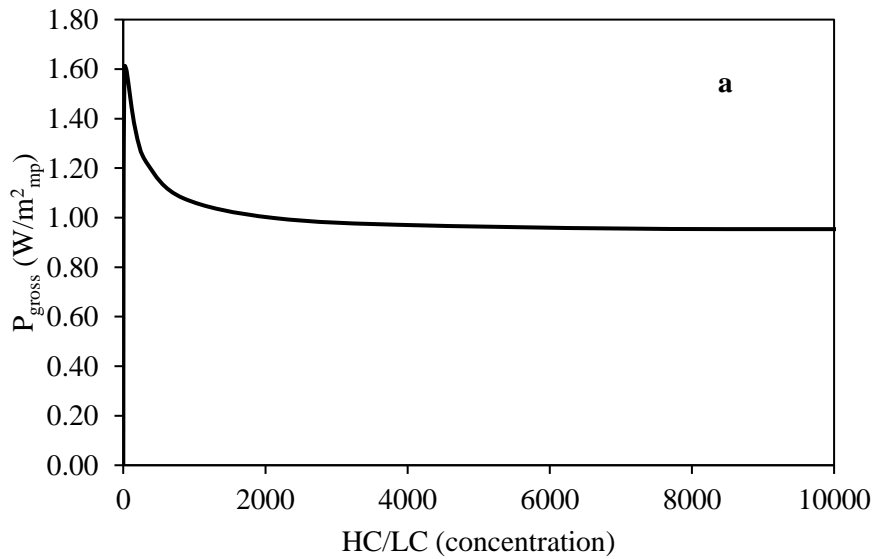
The effect of non-single charged ions in the water streams was not taken into account in this study for the sake of simplicity. According to a previous work studying the effect of non-single charged ions on power performance [20], the trends of the results obtained here could be assimilated for scenarios containing non-single charged ions, with an additional increase in the resistances of the cation and anion ex-change membranes to the same extent, which would translate into a small decrease of gross power up to 8.6 % as maximum, working with seawater as HC.

3. Results and discussion

3.1. The influence of the Low Concentration Solution in energy performance

The concentration of the feed solutions determines the electromotive driving force in RED performance but also has an important effect on the internal resistance of the stacks. Especially, the LC solution, which can be characterized by low values of conductivity, can be a major contributor to the total internal resistance, so that the trade-off between the gain in driving force and the performance lost due to the increase in the internal resistance must be optimized [39]. In order to analyze the influence of the concentration of the LC solution, a parametric sensitivity analysis has been performed in the range from $5.9 \cdot 10^{-5}$ M to 0.5 M NaCl, for a fixed HC solution of 0.55 M NaCl, corresponding to the typical salinity of seawater. Although the superior limit of 0.5 M is not representative of real conditions for LC solutions, since it is very close to the concentration of the HC compartment, it was considered here in order to complete the study over a wide range of concentrations. For this first analysis, the linear flow velocity of both streams were maintained at $1.2 \text{ cm}\cdot\text{s}^{-1}$, which is equivalent to a Reynolds number of 5.4, in line with typical values employed in experimental works [19], and the temperature was set at 24 °C. The minimum resistance values of the IEMS provided by the manufacturer were used for modeling purposes, 0.6 and $1.8 \text{ }\Omega\cdot\text{cm}^2$ for the AEMs and CEMs, respectively. This analysis was accomplished by using a detailed mathematical model implemented in the software Aspen Custom Modeler® [52].

The evolution of gross power and internal resistance of the stack (R_{stack}) as a function of the electromotive driving force defined here as the ratio between HC and LC molar concentrations is displayed in Figure 1, for the range of LC considered. Figure 1.a reflects that gross power output (P) initially increases (see zoom in Figure 1.b) up to an HC/LC ratio of 27.5 in concordance with previous works reported by Long et al. [11,12]. From this point on, the gross power first experiments a sharp drop, and then, beyond HC/LC = 2000, it decreases smoothly. While the electromotive driving force increases, due to an increase in the salinity gradient difference at the expense of reducing the LC concentration, the resistance of the system is affected by the low conductivity of this solution (Figure 1.c) from low HC/LC ratios, as reflected in the loss of power from HC/LC=27.5 (corresponding to an LC concentration of 0.02 M). This can also be seen through the evolution of the overall internal resistance R_{stack} ; after a sharp increase in the internal resistance, R_{stack} tends to smooth down and reach a plateau around $0.20 \Omega \cdot \text{m}^2$ at very high HC/LC ratios.



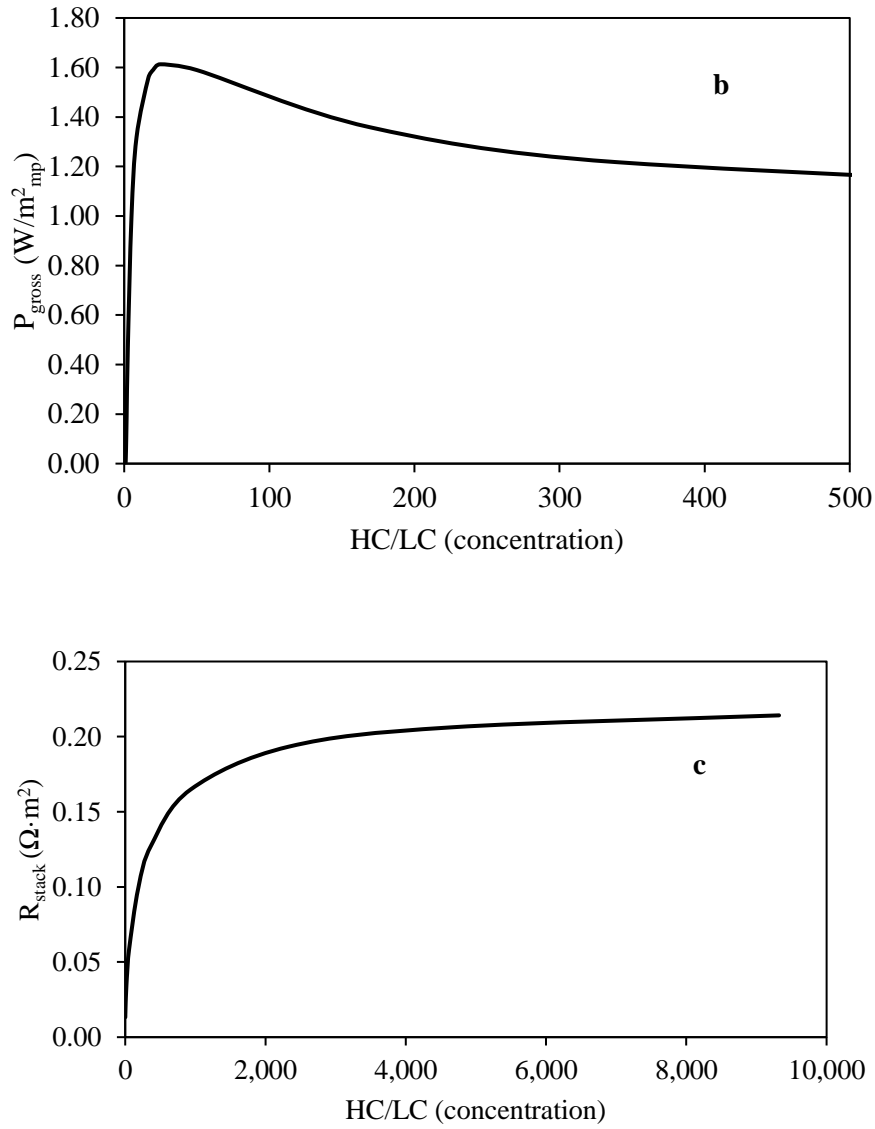


Figure 1. Variation of gross power and R_{stack} as a function of the electromotive driving force using $\text{Re}_{\text{HC}}=\text{Re}_{\text{LC}}=5.4$.

Figure 2.a depicts the open circuit voltage (OCV) of the RED stack as a function of LC concentration keeping constant the Reynold number in both compartments at 5.4. It is observed that OCV decreases as the LC concentration increases according to the Nernst equation, in which lower salinity gradients imply lower OCV values following an exponential decay. For this reason, for an LC concentration of $5.9 \cdot 10^{-5}$ M, a maximum OCV of 5 V was achieved. In contrast, at 0.5 M, when the gradient between LC and HC solutions is close to zero, a minimum OCV of 0.078 V ($0.0039 V_{\text{mp}}$) was obtained. Different behavior is shown for the change in maximum gross power as observed in Figure 2.b. In this case, the gross power reaches a maximum value of 0.65 W for an LC

concentration of 0.02 M (in concordance with the data presented in Figure 1). Moreover, around this optimal concentration, a small region can be observed in which the maximum gross power becomes more stable. This region comprises the LC concentration range between 0.005 M and 0.065 M, as can be observed in the zoom area included in Figure 2.b. Beyond 0.02 M, the salinity gradient decreases as the LC concentration rises, undermining power generation. Below this concentration, although the salinity gradient increases between the LC and HC compartments, the maximum gross power remains below the optimal value due to other parameters affecting the process such as the compartment resistance. For the lowest LC concentration considered of $5.9 \cdot 10^{-5}$ M, only 0.38 W could be reached. In the range from $5.9 \cdot 10^{-5}$ M to 0.02 M, the conductivity of the LC compartments is too low. As it will be quantified later, in this range, the LC compartment resistance displays the highest contribution to the overall internal resistance of the system, causing a reduction in maximum gross power.

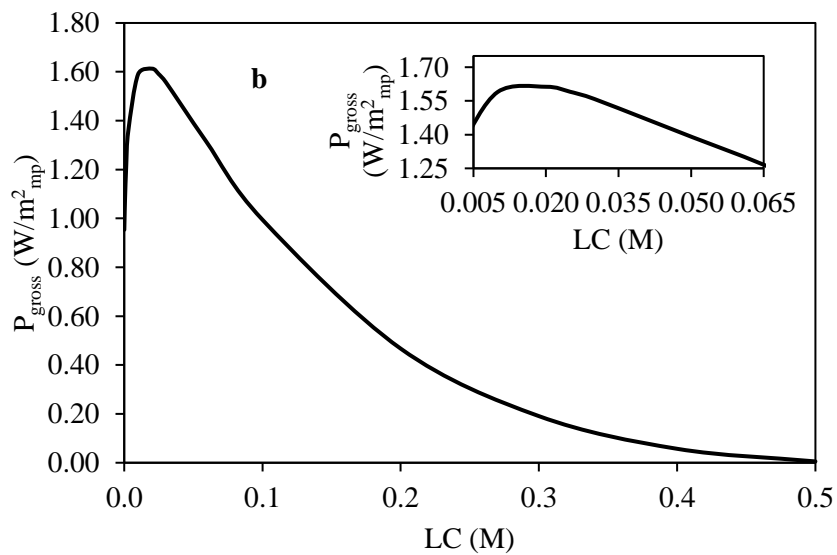
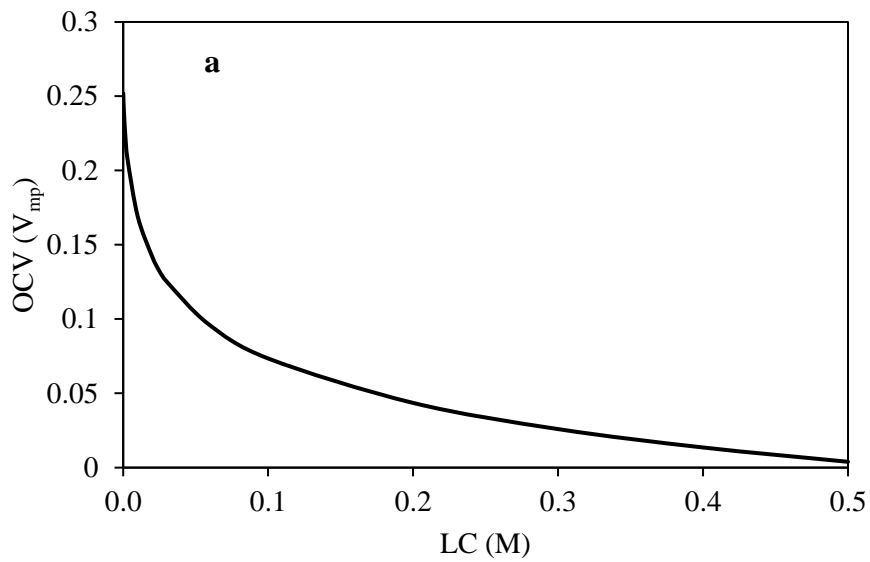


Figure 2. a) OCV_{mp} as a function of LC concentration using $HC=0.55M$; b) Maximum gross power (W/m^2_{mp}) as a function of LC concentration, using $HC=0.55 M$.

The relative contributions offered by the individual resistance components to the total internal resistance of the stack, R_{stack} ($\Omega \cdot \text{m}^2$), are shown in Figure 3. The overall internal resistance can be mainly divided into an ohmic part and a non-ohmic component [21]. Despite of this analysis has been performed for a $\text{Re}_{\text{HC}}=\text{Re}_{\text{LC}}=5.4$, it could be extrapolated to different Reynolds number, without major changes except when extreme velocities are used. In turn, the ohmic resistance is determined by the membrane resistance (R_{m}) and the compartment resistances of the high and low concentration solutions, R_{HC} and R_{LC} , respectively. On the other hand, the non-ohmic part comprises the resistance caused by the concentration change in the bulk solutions along the compartments between inlets and outlets, R_{AC} , and boundary layer resistance, R_{BL} . Specifically, Figure 3.a displays the relative contribution of each resistance type given as a percentage, while Figure 3.b includes the quantitative values of internal resistance. According to these results, when an LC concentration of $5.9 \cdot 10^{-5}$ M was used, the solution resistance displayed a relative contribution of up to 65%. However, this contribution decreases down to 48% for an LC concentration of 0.02 M. It is worth mentioning that the relative contribution of R_{LC} for LC concentrations < 0.059 M always represents the highest relative contribution to the overall internal resistance. It is also noticeable the high relative contributions of R_{AC} from the lowest concentration considered, $5.9 \cdot 10^{-5}$ M, up to 0.059 M. However, for higher LC concentrations (0.5 M), the contributions of the LC compartments and the R_{AC} are lower than that of the membrane resistance (R_{m}).

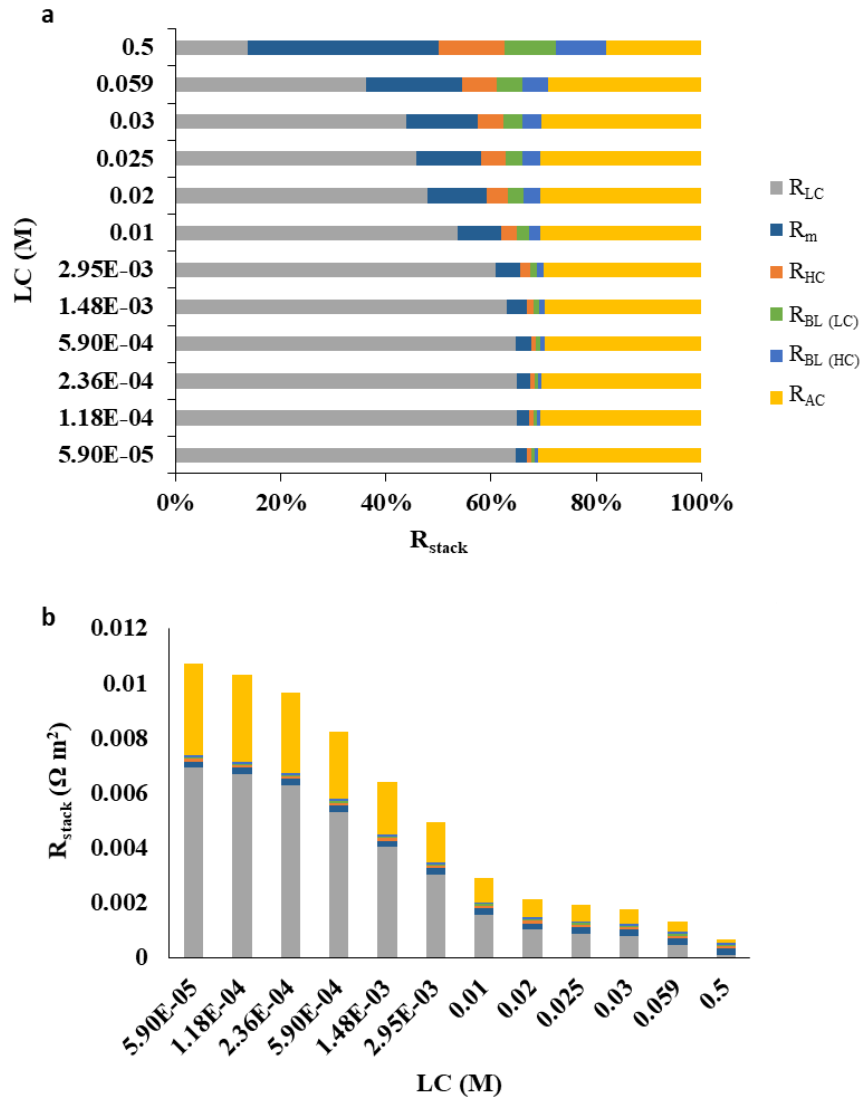


Figure 3. Relative resistance contributions to the total internal resistance (R_{stack}).

Thus, for NaCl concentrations below 0.02 M in the LC compartments, mainly, the high contributions of the R_{LC} and R_{AC} resistances greatly reduce the power output despite the high salinity gradient. The evolution of these two resistance components versus LC concentration is specifically depicted in Figure 4, clearly showing that R_{LC} remains always higher than R_{AC} for the whole range, with exponential decreasing trends in both cases as LC increases.

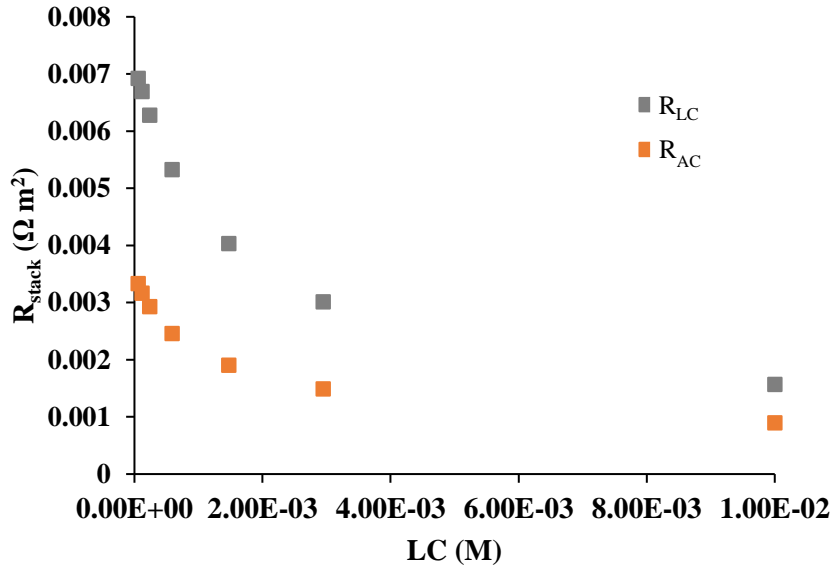


Figure 4. Variation of R_{LC} and R_{AC} as a function of LC concentration ($Re_{HC}=Re_{LC}=5.4$).

According to these results, and considering that 0.02 M would be the optimal concentration for LC solution, a simple and effective strategy towards optimizing the energy performance when using water streams with salt concentrations below this value would consist of mixing such streams with a fraction of seawater. For instance, the salinity of treated wastewater, which can be used as feed stream for LC compartments promoting water reuse and that typically presents lower concentrations, can be increased with a fraction of the HC solution increasing the energy performance of the system up to the value obtained with the optimum LC concentration (0.02 M), as schematically represented in Figure 5.

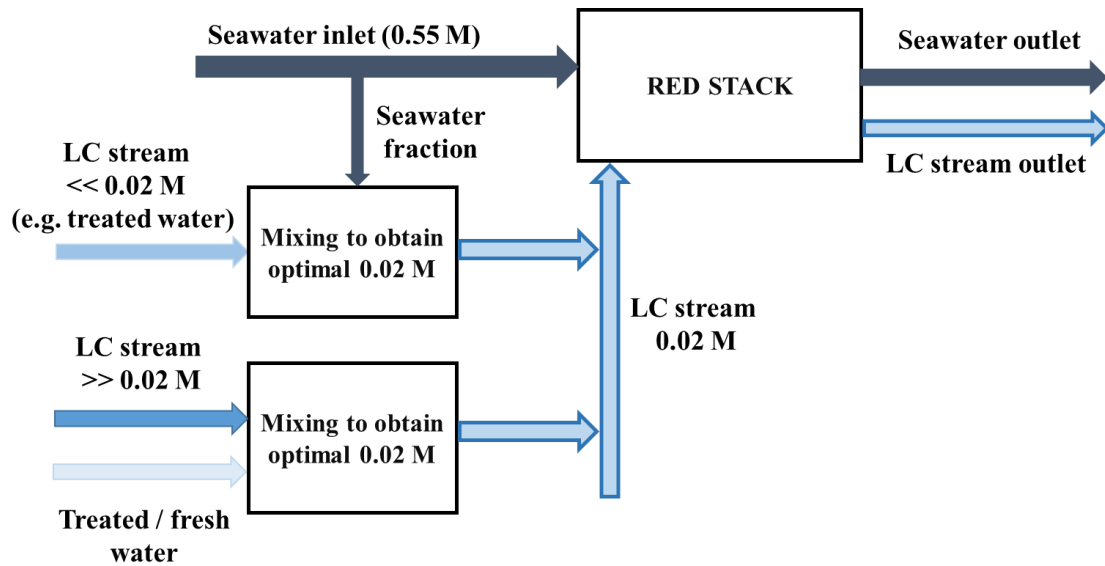


Figure 5. Strategies to adapt LC concentration to optimal values in RED performance.

The robustness of the previously developed mathematical model [52] employed for the sensitivity analysis of the LC concentration was checked with experimental results, in the same conditions as those described for simulation analysis. RED experiments using 0.55 M NaCl as HC solution, corresponding to seawater, and 0.02 M as LC solution, established as optimal concentration for this stream according to the results discussed above, were performed in a laboratory-scale plant. As can be seen in Figures 6 and 7, the experimental values (represented as points) for polarization and power curves are in good agreement with the simulation results. The OCV reached 2.86 V (0.143 V_{mp}) and 2.84 V (0.142 V_{mp}) in experimental and simulation results, respectively. Experimental and simulated gross power curves also overlap as can be observed in Figure 7. Simulation predicted a maximum gross power density value of 1.63 W/m^2_{mp} (normalized to effective pair-cell membrane area), while the experimental maximum gross density was 1.60 W/m^2_{mp} . Thus, the mathematical model validated with these experimental conditions can be used as an optimization tool for RED performance. Moreover, this power density is higher than most of the reported values in RED studies using model waters (only pure NaCl) corresponding to seawater as HC and river water or water treatment plant effluents as LC, and working with similar Re numbers [2,3].

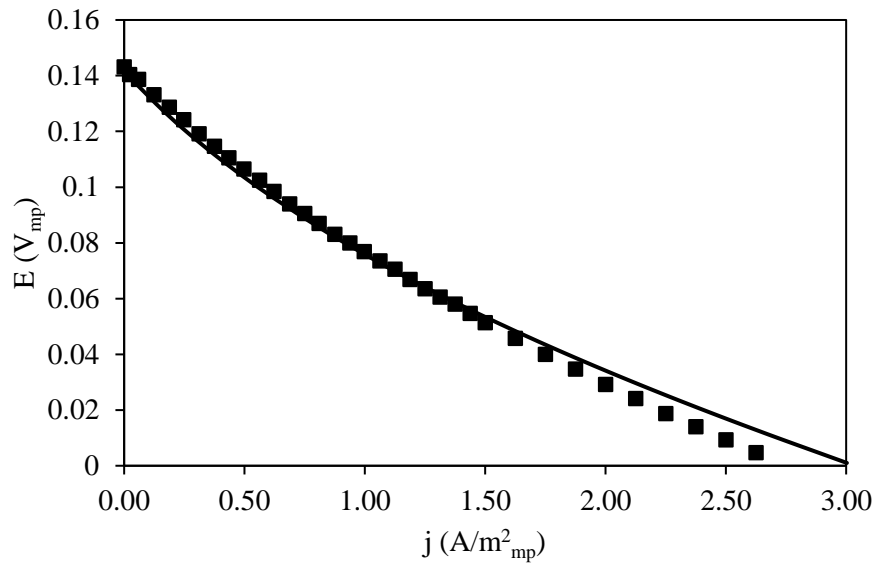


Figure 6. Simulated and experimental results of voltage output (V_{mp}) against current (A/m^2_{mp}).
 $LC=0.02$ M, $HC=0.55$ M. Experimental (points) and simulation (line). $Re_{HC}=Re_{LC}=5.4$.

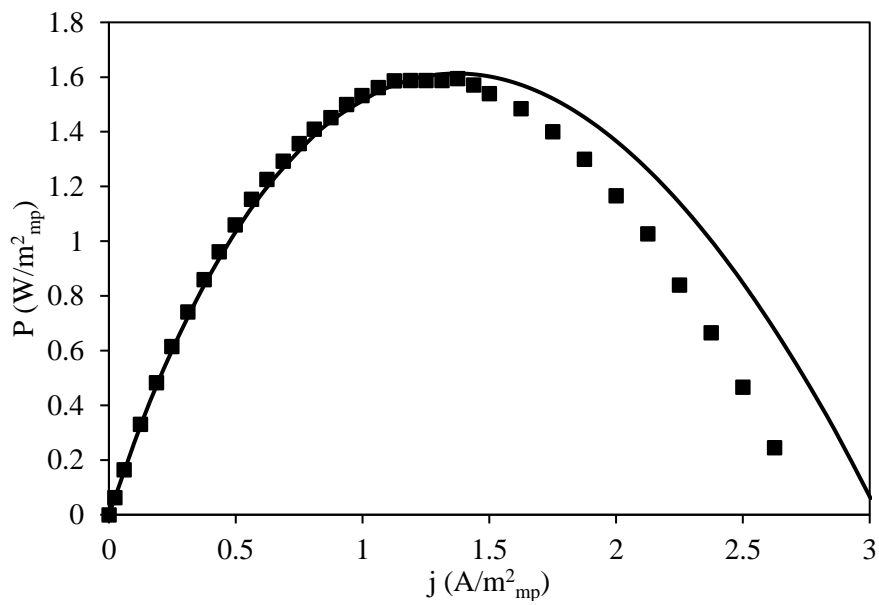


Figure 7. Simulated and experimental results of gross power (W/m^2_{mp}) against current density (A/m^2_{mp}) working with $Re_{HC}=Re_{LC}=5.4$. $LC=0.02$ M, $HC=0.55$ M. Experimental (points) and simulation (line). Std Dev= 0.0148 W/m^2 .

3.2 Sensitivity analysis of the Reynolds number for energy performance optimization

The flow rates of the feed streams strongly affect the power performance in RED systems. The Reynolds number can be used to indicate the fluid dynamic regime inside each compartment in a standard way. Additionally, since it includes the geometry properties of the stack and feed solution properties (viscosity and density), it also allows the comparison between different stack configurations and stream conditions. A parametric analysis of the Reynolds number in both LC and HC compartments was performed using the optimal LC concentration determined in the previous section (LC=0.02 M). Simulations were run for a fixed temperature of 24 °C. Figure 8 shows the curves of gross power as a function of current intensity for values of Re number from 1.4 to 54, but maintained equal in both LC and HC compartments. As it can be observed, gross power increases with Re number. An increase in the Re number implies lower residence times and, therefore, a more uniform concentration gradient throughout the RED stack, with consequently smaller R_{AC} and R_{BL} resistances. Theoretically, the gross power would reach a maximum value when the residence time is zero. It is worth noting that, in this case, pressure drops along the compartments are not considered when estimating gross power. The influence of this parameter is addressed later on for the calculation of the net power.

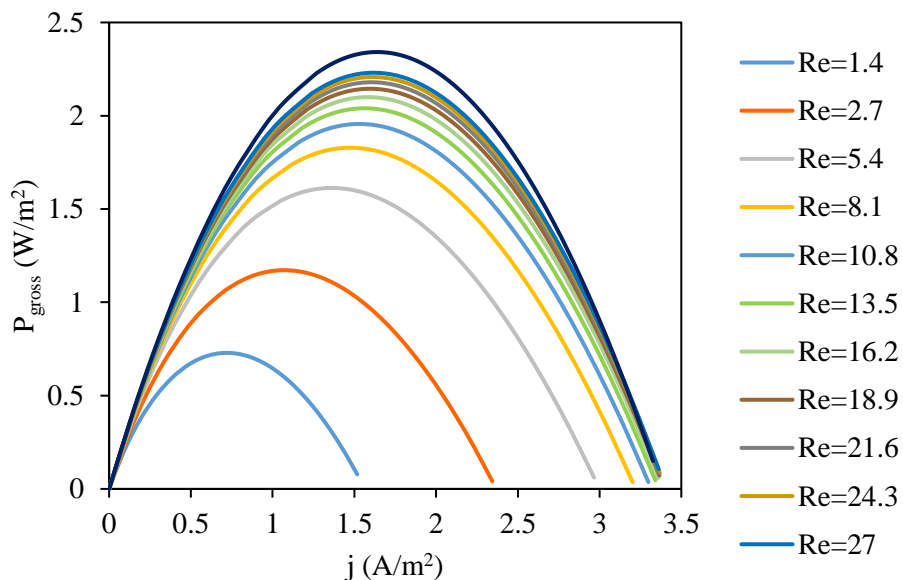


Figure 8. Gross power density as a function of current density at different Re numbers.

$$Re_{HC}=Re_{LC}. HC=0.5 M, LC=0.02 M.$$

To validate the previous results, following a methodology similar to that used in the previous section, experiments working with $Re=10.8$ were performed. Experimentally, the open circuit value was 3 V ($0.15 V_{mp}$), while the predicted simulation value was 2.92 V ($0.146 V_{mp}$). In addition, it can be seen that the slopes of both experimental and simulated polarization curves are in good concordance in Figure 9. Figure 10 displays the corresponding curves of gross power versus current intensity. The experimental and simulated maximum values of gross power density were $1.825 W/m^2_{mp}$ and $1.95W/m^2_{mp}$, respectively, showing that the predictions via simulations were satisfactory.

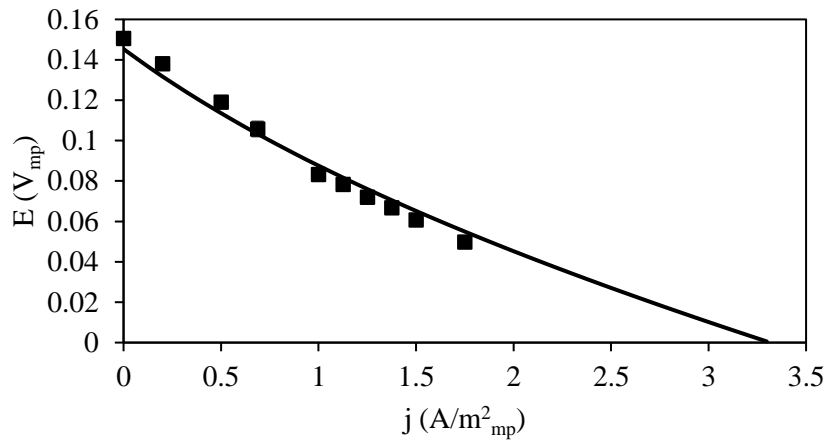


Figure 9. Polarization curve. Experimental (points) and simulated (line) values using $Re_{HC}=Re_{LC}=10.8$.

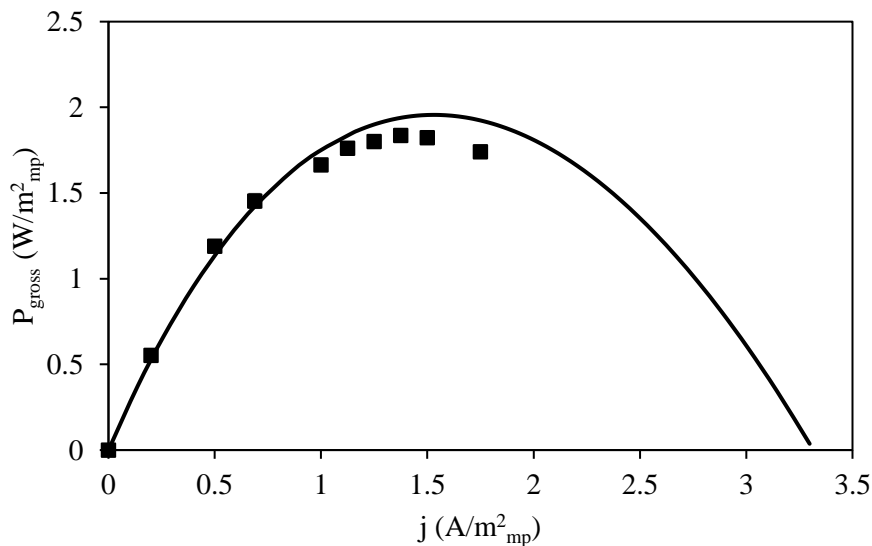


Figure 10. Gross power density versus current density. Experimental (points) and simulated (line) values using $Re_{HC}=Re_{LC}=10.8$. Std Dev= $0.0123 W/m^2$

For the characterization of the energy performance of the RED stack from a practical point of view, net power density can be calculated by subtracting the power spent in fluids pumping from gross power [47], according to the equation 4, included in the section of Materials and Methods, which takes into consideration the pressure drops along the compartments. Figure 11 shows the change of gross power, net power and pump consumption as a function of the Reynolds number working with the following conditions: (i) the same Re number in the HC and LC solutions (Figure 11.a) and (ii) maintaining constant the Re number ($Re=5.4$) in one of the solutions while varying the other (Figure 11.b-11.c). For these three cases, several overall trends can be observed.

On one hand, pump consumption and maximum gross power increased potentially with the Reynolds number and thus with flow rates. On the other hand, net power increases up to a maximum and decreases thereafter because, from such point on, the increase in gross power is lower than pumping power consumption. However, delving into the differences between the scenarios b and c, it can be observed that the maximum net power is achieved at a higher value of Re_{LC} , when the Re_{HC} is maintained constant ($Re_{HC}=5.4$). Specifically working with a $Re_{LC}=6.75$ a net power value of 0.526 W was accomplished (scenario b). Besides, the range of the Reynolds number in which net power can be improved is wider for the Re_{LC} in comparison to the Re_{HC} . Thus, when Re_{LC} is maintained constant ($Re_{LC}=5.4$) a value of 0.631 W using a $Re_{HC}=4$ was obtained (scenario c).

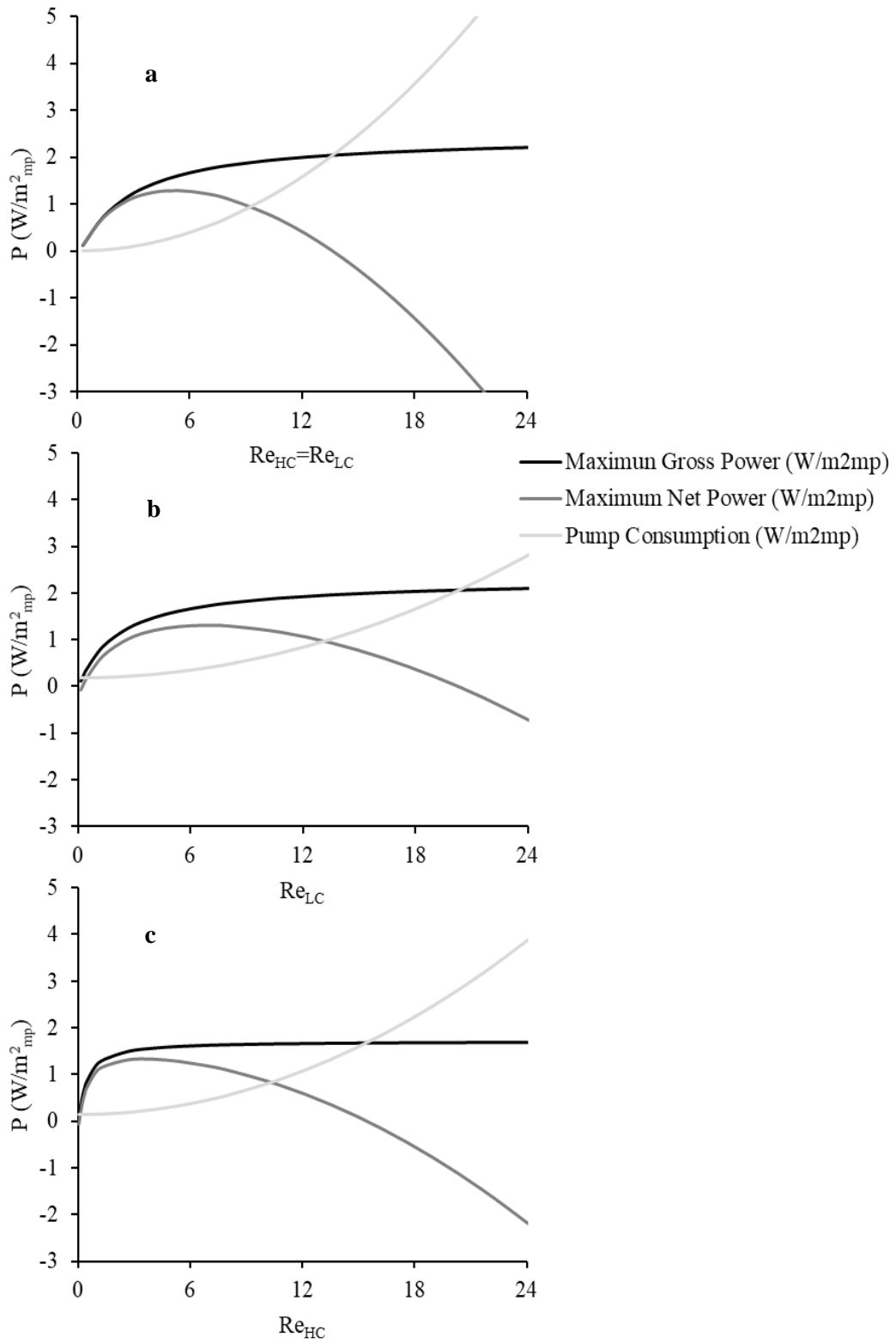


Figure 11. Evolution of gross power, net power and pump consumption (W/m^2_{mp}) as a function of the Re number: a) $Re_{HC} = Re_{LC}$, b) Re_{LC} , c) Re_{HC}

A contour graph of the maximum net power as a function of Re number was plotted by using the results of net power (Figure 12). An optimal net power value of 0.545 W (1.35 W/m²) was obtained working with Re_{HC}=3.4 and Re_{LC}=7. These Reynolds values are within the recommended ranges reported in the literature (Re<10) [37,42,43,54]. Thus, it can be concluded that, in general, when higher values of Re_{LC} than Re_{HC} numbers are used, they have a positive effect on net power. Another important observation is that small changes in terms of Re in the HC compartment imply higher changes in the net power.

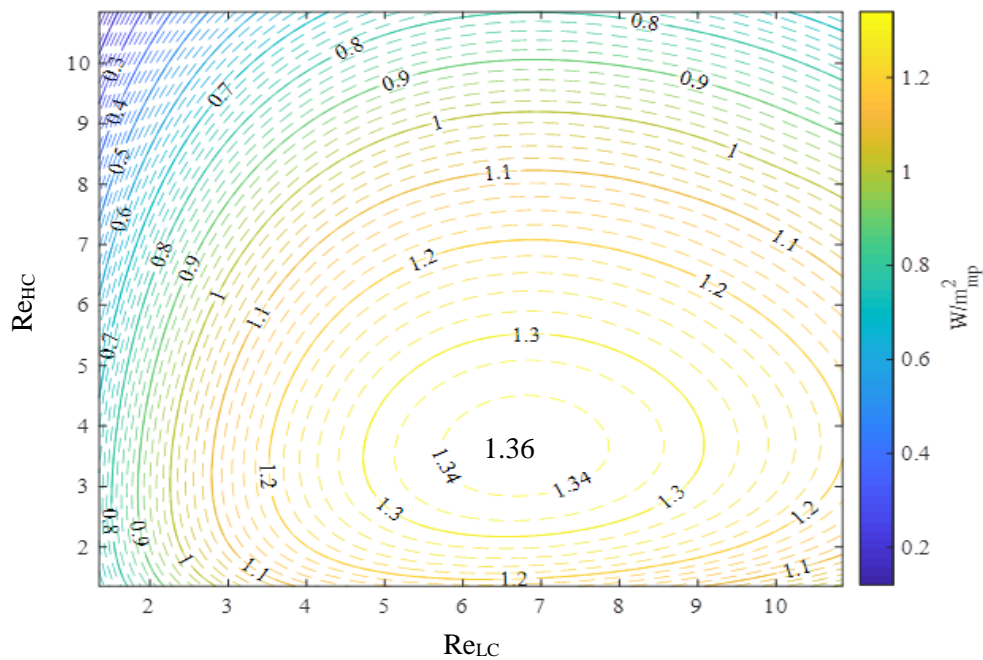


Figure 12. Contour graph of net power as a function of the Re numbers.

As previously mentioned, it must be noted that the presence of non-single charged ions in the feeding water streams has not been considered. This issue was already addressed in a previous reported work [17], showing that divalent ions contribute to the increase of the internal resistance by raising the resistance of the cation and anion exchange membranes. This would translate into a decrease in power output to some extent. Specifically, when non-single charged ions are added at realistic concentrations, a small reduction of up to 8.6% in gross power is observed working with seawater as HC [20]. Thus, it can be assumed that the trends of the results obtained would be valid when considering the possible presence of non-single charged ions. Figure 13 shows a flow

diagram in order to summarize the inputs required to predict RED performance under different scenarios, operational variables and RED stack features.

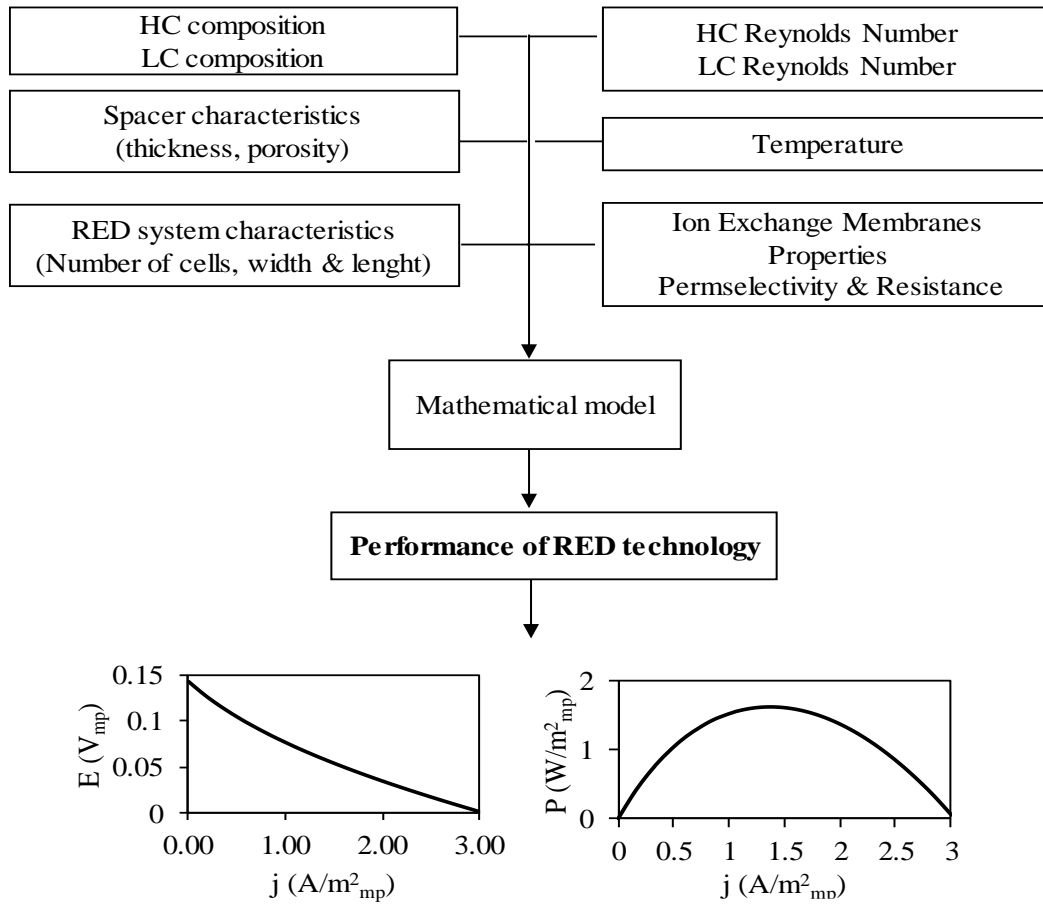


Figure 13. Flow diagram to predict RED performance.

Conclusions

The large-scale implementation of RED technology goes through the optimization of the main variables involved in the process, from design parameters such as membrane and spacer configuration to operation variables, including stream concentrations and flow rates in the compartments. In this last case, the selection of the LC stream and feed flow rates offer different trade-offs that can be assessed using modeling approaches. This work presents the parametric analyses of the LC salinity and the feed flow rates, in terms of the Reynolds number in the HC and LC compartments, using a previously developed mathematical model; the concentration of HC solution has been maintained at 0.55 M NaCl, which corresponds to the typical salinity of seawater with global availability for SGP exploitation. For such concentration, the influence of the HC resistance is low. The

relative contributions of the non-ohmic and ohmic components to the overall internal resistance of the system were quantified as a function of LC concentration. According to the parametric analysis performed, the resistance of the LC compartment offers the greatest relative contribution to the total overall internal resistance of the RED stack. In addition, an optimal concentration in the region around 0.02 M was found for the LC solution. On the other hand, the parametric analysis of the Reynolds number allowed the study of the individual influences of feed flows in HC and LC compartments, as well as, the interaction between them for the optimization of RED performance. In this regard, it was demonstrated that the use of higher values of Re_{LC} in comparison to Re_{HC} has a positive effect on net power. Moreover, small changes in the Re_{HC} imply higher changes in net power. The mathematical model was thus employed as an optimization tool, validated with experimental conditions. The analysis of the effect of the LC concentrations provided in this work, makes a step forward in the design and optimization of RED technology; it can help to make a proper selection of the water streams to be used as well as to design new strategies for adapting the available ones, e.g. by increasing the salinity of available water sources to the optimal salt concentration (0.02 M) with a fraction of the HC solution. Moreover, the Reynolds number can be used to confront different configuration stacks and water streams for comparative purposes and upscaling.

Nomenclature

I	Current (A)
j	Current density (A/m^2)
b	Spacer thickness
MP	Membrane Pair
P	Power density (W/m^2)
$R_{\Delta C}$	Concentration change in the bulk solution Resistance ($\Omega \cdot m^2$)
R_{AEM}	Anionic Membrane Resistance ($\Omega \cdot m^2$)
R_{BL}	Boundary Layer Resistance ($\Omega \cdot m^2$)
R_{CEM}	Cationic Membrane Resistance ($\Omega \cdot m^2$)
Re	Reynolds number

R_{HC}	High Concentration Solution Resistance ($\Omega \cdot m^2$)
R_{stack}	Overall Internal Resistance ($\Omega \cdot m^2$)
R_L	External Load Resistance ($\Omega \cdot m^2$)
R_{LC}	Low Concentration Solution Resistance ($\Omega \cdot m^2$)
R_{mem}	Average Membrane Resistance ($\Omega \cdot m^2$)
$R_{non-ohmic}$	Non-ohmic Resistance ($\Omega \cdot m^2$)
R_{ohmic}	Ohmic Resistance ($\Omega \cdot m^2$)
E	Voltage (V)

Abbreviation

AEM	Anion Exchange Membrane
CEM	Cation Exchange Membrane
ERS	Electrode Rinse Solution
IEM	Ion Exchange Membrane
OCV	Open Circuit Voltage
PRO	Pressure Retarded Osmosis
RED	Reverse Electrodialysis
SGP	Salinity Gradient Power
WWTP	Wastewater Treatment Plant

Subscript

HC	High Concentrated Solution
LC	Low Concentrated Solution
MP	Membrane Pair

Acknowledgements

This work has been performed within financial support from Community of Cantabria - Regional Plan for the project: Gradisal “RM16-XX-046-SODERCAN/FEDER”. Moreover, authors acknowledge Spanish Ministry of Economy and Competitiveness for the projects CTM2014-57833-R and CTM2017-87850-R. This research is being supported by the Project “HYLANTIC”- EAPA_204/2016, which is co-financed by the European Regional Development Fund in the framework of the Interreg Atlantic program. V.M. Ortiz-Martínez is supported by the Spanish Ministry of Science, Innovation and Universities (grant ‘Juan de la Cierva-Formación’ ref. FJCI-2017-32404).

References

- [1] E. Farrell, M.I. Hassan, R.A. Tufa, A. Tuomiranta, A.H. Avci, A. Politano, E. Curcio, H.A. Arafat, Reverse electrodialysis powered greenhouse concept for water- and energy-self-sufficient agriculture, *Appl. Energy*. 187 (2017) 390–409. doi:10.1016/j.apenergy.2016.11.069.
- [2] R.A. Tufa, S. Pawlowski, J. Veerman, K. Bouzek, E. Fontananova, G. di Profio, S. Velizarov, J. Goulão Crespo, K. Nijmeijer, E. Curcio, Progress and prospects in reverse electrodialysis for salinity gradient energy conversion and storage, *Appl. Energy*. 225 (2018) 290–331. doi:10.1016/j.apenergy.2018.04.111.
- [3] Y. Mei, C.Y. Tang, Recent developments and future perspectives of reverse electrodialysis technology: A review, *Desalination*. 425 (2017) 156–174. doi:10.1016/j.desal.2017.10.021.
- [4] J.W. Post, J. Veerman, H.V.M. Hamelers, G.J.W. Euverink, S.J. Metz, K. Nijmeijer, C.J.N. Buisman, Salinity-gradient power: Evaluation of pressure-retarded osmosis and reverse electrodialysis, *J. Memb. Sci.* 288 (2007) 218–230. doi:10.1016/j.memsci.2006.11.018.
- [5] J. Veerman, M. Saakes, S.J. Metz, G.J. Harmsen, Reverse electrodialysis: Performance of a stack with 50 cells on the mixing of sea and river water, *J. Memb. Sci.* 327 (2009) 136–144. doi:10.1016/j.memsci.2008.11.015.
- [6] A. Achilli, A.E. Childress, Pressure retarded osmosis: From the vision of Sidney

- Loeb to the first prototype installation - Review, *Desalination*. 261 (2010) 205–211. doi:10.1016/j.desal.2010.06.017.
- [7] J. Veerman, D.A. Vermaas, *Reverse electrodialysis: Fundamentals*, Elsevier Ltd., 2016. doi:10.1016/B978-0-08-100312-1.00004-3.
- [8] E. Curcio, G. Di Profio, E. Fontananova, E. Drioli, *Membrane technologies for seawater desalination and brackish water treatment*, 2015. doi:10.1016/B978-1-78242-121-4.00013-7.
- [9] M. Reig, H. Farrokhzad, B. Van der Bruggen, O. Gibert, J.L. Cortina, Synthesis of a monovalent selective cation exchange membrane to concentrate reverse osmosis brines by electrodialysis, *Desalination*. (2015). doi:10.1016/j.desal.2015.07.023.
- [10] A. Zlotorowicz, R. V. Strand, O.S. Burheim, Wilhelmsen, S. Kjelstrup, The permselectivity and water transference number of ion exchange membranes in reverse electrodialysis, *J. Memb. Sci.* (2017). doi:10.1016/j.memsci.2016.10.003.
- [11] R. Long, B. Li, Z. Liu, W. Liu, Performance analysis of reverse electrodialysis stacks: Channel geometry and flow rate optimization, *Energy*. 158 (2018) 427–436. doi:10.1016/j.energy.2018.06.067.
- [12] R. Long, B. Li, Z. Liu, W. Liu, Reverse electrodialysis: Modelling and performance analysis based on multi-objective optimization, *Energy*. 151 (2018) 1–10. doi:10.1016/j.energy.2018.03.003.
- [13] S. Mehdizadeh, M. Yasukawa, T. Abo, Y. Kakihana, M. Higa, Effect of spacer geometry on membrane and solution compartment resistances in reverse electrodialysis, *J. Memb. Sci.* (2019). doi:10.1016/j.memsci.2018.09.051.
- [14] H.K. Kim, M.S. Lee, S.Y. Lee, Y.W. Choi, N.J. Jeong, C.S. Kim, High power density of reverse electrodialysis with pore-filling ion exchange membranes and a high-open-area spacer, *J. Mater. Chem. A*. (2015). doi:10.1039/c5ta03571f.
- [15] J. Veerman, M. Saakes, S.J. Metz, G.J. Harmsen, *Reverse electrodialysis: Evaluation of suitable electrode systems*, *J. Appl. Electrochem.* (2010). doi:10.1007/s10800-010-0124-8.
- [16] O. Scialdone, C. Guarisco, S. Grispo, A.D. Angelo, A. Galia, Investigation of electrode material - Redox couple systems for reverse electrodialysis processes.

- Part I: Iron redox couples, *J. Electroanal. Chem.* (2012). doi:10.1016/j.jelechem.2012.05.017.
- [17] S. Mehdizadeh, M. Yasukawa, M. Kuno, Y. Kawabata, M. Higa, Evaluation of energy harvesting from discharged solutions in a salt production plant by reverse electrodialysis (RED), *Desalination*. (2019). doi:10.1016/j.desal.2019.04.007.
- [18] M. Micari, M. Bevacqua, A. Cipollina, A. Tamburini, W. Van Baak, T. Putts, G. Micale, Effect of different aqueous solutions of pure salts and salt mixtures in reverse electrodialysis systems for closed-loop applications, *J. Memb. Sci.* (2018). doi:10.1016/j.memsci.2018.01.036.
- [19] D.A. Vermaas, J. Veerman, M. Saakes, K. Nijmeijer, Influence of multivalent ions on renewable energy generation in reverse electrodialysis, *Energy Environ. Sci.* 7 (2014) 1434–1445. doi:10.1039/C3EE43501F.
- [20] L. Gómez-Coma, V.M. Ortiz-Martínez, J. Carmona, L. Palacio, P. Prádanos, M. Fallanza, A. Ortiz, R. Ibañez, I. Ortiz, Modeling the influence of divalent ions on membrane resistance and electric power in reverse electrodialysis, *J. Memb. Sci.* 592 (2019) 117385. doi:10.1016/j.memsci.2019.117385.
- [21] X. Zhu, W. He, B.E. Logan, Reducing pumping energy by using different flow rates of high and low concentration solutions in reverse electrodialysis cells, *J. Memb. Sci.* 486 (2015) 215–221. doi:10.1016/j.memsci.2015.03.035.
- [22] S. Mehdizadeh, M. Yasukawa, T. Abo, M. Kuno, Y. Noguchi, M. Higa, The Effect of Feed Solution Temperature on the Power Output Performance of a Pilot-Scale Reverse Electrodialysis (RED) System with Different Intermediate Distance, Membranes (Basel). (2019). doi:10.3390/membranes9060073.
- [23] A.M. Benneker, T. Rijnaarts, R.G.H. Lammertink, J.A. Wood, Effect of temperature gradients in (reverse) electrodialysis in the Ohmic regime, *J. Memb. Sci.* (2018). doi:10.1016/j.memsci.2017.11.029.
- [24] J. Hu, S. Xu, X. Wu, D. Wu, D. Jin, P. wang, Q. Leng, Multi-stage reverse electrodialysis: Strategies to harvest salinity gradient energy, *Energy Convers. Manag.* (2019). doi:10.1016/j.enconman.2018.11.032.
- [25] J. Choi, Y. Oh, S. Chae, S. Hong, Membrane capacitive deionization-reverse

- electrodialysis hybrid system for improving energy efficiency of reverse osmosis seawater desalination, *Desalination*. (2019). doi:10.1016/j.desal.2019.04.003.
- [26] J. Hu, S. Xu, X. Wu, D. Wu, D. Jin, P. Wang, L. Xu, Q. Leng, Exergy analysis for the multi-effect distillation - reverse electrodialysis heat engine, *Desalination*. (2019). doi:10.1016/j.desal.2019.06.007.
- [27] M. Tedesco, C. Scalici, D. Vaccari, A. Cipollina, A. Tamburini, G. Micale, Performance of the first reverse electrodialysis pilot plant for power production from saline waters and concentrated brines, *J. Memb. Sci.* 500 (2016) 33–45. doi:10.1016/j.memsci.2015.10.057.
- [28] M. Tedesco, A. Cipollina, A. Tamburini, G. Micale, Towards 1 kW power production in a reverse electrodialysis pilot plant with saline waters and concentrated brines, *J. Memb. Sci.* 522 (2017) 226–236. doi:10.1016/j.memsci.2016.09.015.
- [29] A. Cipollina, G. Micale, A. Tamburini, M. Tedesco, L. Gurreri, J. Veerman, S. Grasman, *Reverse electrodialysis: Applications*, Elsevier Ltd., 2016. doi:10.1016/B978-0-08-100312-1.00005-5.
- [30] L. Gómez-Coma, V.M. Ortiz-Martínez, M. Fallanza, A. Ortiz, R. Ibañez, I. Ortiz, Blue energy for sustainable water reclamation in WWTPs, *J. Water Process Eng.* 33 (2020) 101020. doi:10.1016/j.jwpe.2019.101020.
- [31] J.G. Hong, B. Zhang, S. Glabman, N. Uzal, X. Dou, H. Zhang, X. Wei, Y. Chen, Potential ion exchange membranes and system performance in reverse electrodialysis for power generation: A review, *J. Memb. Sci.* 486 (2015) 71–88. doi:10.1016/j.memsci.2015.02.039.
- [32] M. Tedesco, A. Cipollina, A. Tamburini, W. van Baak, G. Micale, Modelling the Reverse ElectroDialysis process with seawater and concentrated brines, *Desalin. Water Treat.* 49 (2012) 404–424. doi:10.1080/19443994.2012.699355.
- [33] J. Gi Hong, Y. Chen, Evaluation of electrochemical properties and reverse electrodialysis performance for porous cation exchange membranes with sulfate-functionalized iron oxide, *J. Memb. Sci.* 473 (2015) 210–217. doi:10.1016/j.memsci.2014.09.012.

- [34] G.M. Geise, M.A. Hickner, B.E. Logan, Ionic Resistance and Permselectivity Tradeoffs in Anion Exchange Membranes, *ACS Appl. Mater. Interfaces*. 5 (2013) 10294–10301. doi:10.1021/am403207w.
- [35] E. Güler, W. van Baak, M. Saakes, K. Nijmeijer, Monovalent-ion-selective membranes for reverse electrodialysis, *J. Memb. Sci.* (2014). doi:10.1016/j.memsci.2013.12.054.
- [36] D.A. Vermaas, M. Saakes, K. Nijmeijer, Enhanced mixing in the diffusive boundary layer for energy generation in reverse electrodialysis, *J. Memb. Sci.* 453 (2014) 312–319. doi:10.1016/j.memsci.2013.11.005.
- [37] D.A. Vermaas, M. Saakes, K. Nijmeijer, Power generation using profiled membranes in reverse electrodialysis, *J. Memb. Sci.* 385–386 (2011) 234–242. doi:10.1016/j.memsci.2011.09.043.
- [38] P. Długole, A. Gambier, M. Wessling, Practical Potential of Reverse Electrodialysis As Process for Sustainable Energy Generation, 43 (2009) 6888–6894.
- [39] A. Daniilidis, D.A. Vermaas, R. Herber, K. Nijmeijer, Experimentally obtainable energy from mixing river water, seawater or brines with reverse electrodialysis, *Renew. Energy*. 64 (2014) 123–131. doi:10.1016/j.renene.2013.11.001.
- [40] Y. Mei, C.Y. Tang, Co-locating reverse electrodialysis with reverse osmosis desalination: Synergies and implications, *J. Memb. Sci.* (2017). doi:10.1016/j.memsci.2017.06.014.
- [41] M. Tedesco, A. Cipollina, A. Tamburini, I.D.L. Bogle, G. Micale, A simulation tool for analysis and design of reverse electrodialysis using concentrated brines, *Chem. Eng. Res. Des.* 93 (2015) 441–456. doi:10.1016/j.cherd.2014.05.009.
- [42] D.A. Vermaas, M. Saakes, K. Nijmeijer, Doubled power density from salinity gradients at reduced intermembrane distance, *Environ. Sci. Technol.* 45 (2011) 7089–7095. doi:10.1021/es2012758.
- [43] M. Tedesco, E. Brauns, A. Cipollina, G. Micale, P. Modica, G. Russo, J. Helsen, Reverse electrodialysis with saline waters and concentrated brines: A laboratory investigation towards technology scale-up, *J. Memb. Sci.* 492 (2015) 9–20.

doi:10.1016/j.memsci.2015.05.020.

- [44] A. Daniilidis, R. Herber, D.A. Vermaas, Upscale potential and financial feasibility of a reverse electro dialysis power plant, *Appl. Energy*. 119 (2014) 257–265. doi:10.1016/j.apenergy.2013.12.066.
- [45] J.W. Post, H.V.M. Hamelers, C.J.N. Buisman, Energy recovery from controlled mixing salt and fresh water with a reverse electro dialysis system, *Environ. Sci. Technol.* 42 (2008) 5785–5790. doi:10.1021/es8004317.
- [46] G.J.A.N. Harmsen, Electrical Power from Sea and River Water by Reverse Electro dialysis : A First Step from the Laboratory to a Real Power Plant, 44 (2010) 9207–9212.
- [47] S. Pawlowski, J.G. Crespo, S. Velizarov, Pressure drop in reverse electro dialysis: Experimental and modeling studies for stacks with variable number of cell pairs, *J. Memb. Sci.* 462 (2014) 96–111. doi:10.1016/j.memsci.2014.03.020.
- [48] R.A. Tufa, E. Curcio, W. van Baak, J. Veerman, S. Grasman, E. Fontananova, G. Di Profio, Potential of brackish water and brine for energy generation by salinity gradient power-reverse electro dialysis (SGP-RE), *RSC Adv.* 4 (2014) 42617–42623. doi:10.1039/C4RA05968A.
- [49] R.S. Kingsbury, F. Liu, S. Zhu, C. Boggs, M.D. Armstrong, D.F. Call, O. Coronell, Impact of natural organic matter and inorganic solutes on energy recovery from five real salinity gradients using reverse electro dialysis, *J. Memb. Sci.* 541 (2017) 621–632. doi:10.1016/j.memsci.2017.07.038.
- [50] Y.M. Chao, T.M. Liang, A feasibility study of industrial wastewater recovery using electro dialysis reversal, *Desalination*. 221 (2008) 433–439. doi:10.1016/j.desal.2007.04.065.
- [51] R.A. Tufa, E. Curcio, E. Brauns, W. van Baak, E. Fontananova, G. Di Profio, Membrane Distillation and Reverse Electro dialysis for Near-Zero Liquid Discharge and low energy seawater desalination, *J. Memb. Sci.* 496 (2015) 325–333. doi:10.1016/j.memsci.2015.09.008.
- [52] R. Ortiz-imediao, L. Gomez-coma, M. Fallanza, A. Ortiz, R. Ibañez, I. Ortiz, Comparative performance of Salinity Gradient Power-Reverse Electro dialysis

- under different operating conditions, *Desalination*. 457 (2019) 8–21. doi:10.1016/j.desal.2019.01.005.
- [53] J. Veerman, M. Saakes, S.J. Metz, G.J. Harmsen, Reverse electrodialysis: A validated process model for design and optimization, *Chem. Eng. J.* 166 (2011) 256–268. doi:10.1016/j.cej.2010.10.071.
- [54] D.A. Vermaas, E. Guler, M. Saakes, K. Nijmeijer, Theoretical power density from salinity gradients using reverse electrodialysis, *Energy Procedia*. 20 (2012) 170–184. doi:10.1016/j.egypro.2012.03.018.

Supplementary Material

RED stack specifications

The main specifications of the RED stack employed in the experimental set-up is included in Table S1.

Table S1. RED stack specifications

	Value
Area of one membrane (m ²)	0.02
Cell width (m)	0.063
Cell length (m)	0.32
Intermembrane distance (m)	$5 \cdot 10^{-5}$
Membrane pairs	20
AEM permselectivity (0.1-0.5 M)	0.92-0.96
CEM permselectivity (0.1-0.5 M)	0.97-0.99
AEM resistance ($\Omega \cdot \text{cm}^2$)*	0.6-1.5
CEM resistance ($\Omega \cdot \text{cm}^2$)*	1.8-2.5
Spacers thickness (μm)	270

*0.5 M NaCl, T = 298 K

Schematic representation of RED stack

Figure S1 presents a schematic representation of the laboratory plant setup used in this work.

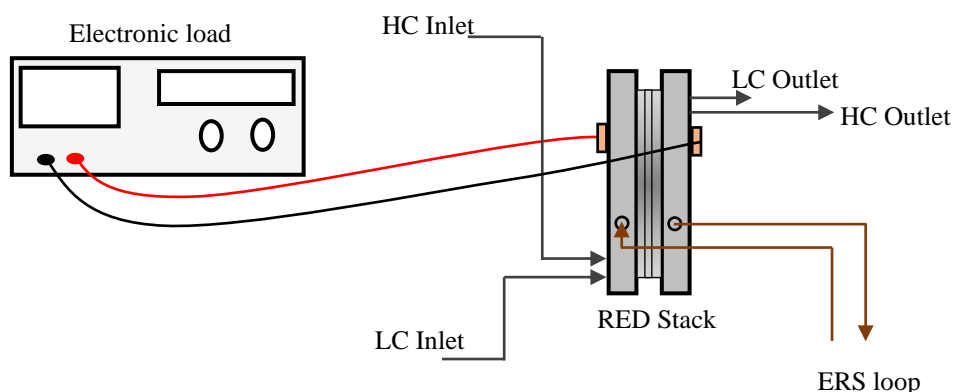


Figure S1. Schematic of the experimental set-up.